

Metrologically useful states of spin-1 Bose condensates with macroscopic magnetization

Dariusz Kajtoch,¹ Krzysztof Pawłowski² and Emilia Witkowska¹

¹*Institute of Physics, PAS, Aleja Lotników 32/46, PL-02668 Warsaw, Poland*

²*Center for Theoretical Physics, PAS, Aleja Lotników 32/46, PL-02668 Warsaw, Poland*

(Dated: December 3, 2024)

We study theoretically usability of spin-1 Bose condensates with nonzero magnetization in a homogeneous magnetic field for quantum metrology. We demonstrate Heisenberg scaling of the quantum Fisher information for states in thermal equilibrium, including the zero temperature case. It applies to both anti-ferromagnetic and ferromagnetic interactions. The effect preserves as long as fluctuations of magnetization are sufficiently small. Scaling of the quantum Fisher information with the total particle number is derived within the mean-field limit at zero temperature and exactly in the high magnetic field limit for any temperature. The precision gain is intuitively explained owing to subtle features of the quasi-distribution function in phase space.

PACS numbers: 03.67.Bg, 03.75.Dg, 03.75.Gg.

Atom interferometry techniques are widely used in most precise measurements of physical parameters e.g. time, force or strength of a field. The physical quantities are typically mapped onto a phase θ which is estimated afterwards. The best precision in the θ estimation is limited by the Cramér-Rao bound $\Delta\theta \gtrsim F_Q^{-1/2}$ [1], where F_Q is the quantum Fisher information (QFI). When N uncorrelated atoms are used, the best precision is given by the standard quantum limit (SQL) with $F_Q \sim N$ resulting from the statistical nature of quantum noise. The SQL can be beaten using quantum resources such as squeezing and entanglement, potentially approaching the ultimate Heisenberg limit $F_Q \sim N^2$. The class of useful for interferometry entangled states is fully identified by the QFI which quantifies potential improvement in the precision of the θ estimation. The QFI is a witness for genuinely multi-particle entanglement [2–4]. It is also interpreted as a statistical speed of changes of an output state of a linear interferometer under an infinitesimal increment of θ [5]. This geometrical interpretation of the QFI provides an experimental tool to extract the Fisher information [6]. Additionally, the QFI is related to dynamical susceptibilities [7] which can also be measured in experiments.

Multicomponent Bose-Einstein condensates (BECs) of ultra-cold atoms have been already recognized as realistic systems of highly controllable and tunable systems for entangled states generation [6–14] useful for atomic interferometry. Here, we concentrate on anti-ferromagnetic and ferromagnetic spin-1 Bose condensates for the situation of current experimental relevance [13], where N is large and the magnetization of the system M (population difference of extreme Zeeman levels) is conserved. Entanglement in the system is investigated experimentally nowadays [14–17], including observation of twin-Fock states [16, 17], however for zero magnetization. In the Letter we show that thermal states of the system with macroscopic magnetization, i.e. $M = O(N)$ and $N - M = O(N)$, are highly entangled for a wide range of magnetic fields and interaction strengths.

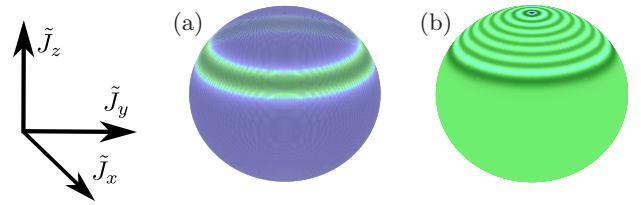


FIG. 1. (Color online) Illustration of the Husimi (a) and Wigner (b) quasi-distribution functions for eigenstates of the system: an example for the state $|(N + M)/2, (N - M)/2\rangle$ with $N = 60$, $M = N/2$.

By performing numerical calculations of the QFI within the exact diagonalization method, we make a quite interesting observation. Thermal states of the system provide Heisenberg scaling of the QFI as long as the variance of magnetization is below one. The resulting scaling can be intuitively understood by considering the Wigner [18] quasi-distribution in appropriate $SU(2)$ sub-algebras, as illustrated in Fig.1. The Wigner functions of the system’s eigenstates, which can be approximated by the Fock states, form parallel rings of width N times smaller than the size of the whole Bloch sphere. Heuristically, this implies very fast changes of the state due to rotation around any axis in the $x - y$ plane of the corresponding Bloch sphere, giving rise to Heisenberg scaling of the QFI. However, fluctuations of magnetization larger than one smear out narrow structures in the corresponding quasi-distributions, resulting in decrease of the QFI with rate inversely proportional to the variance of magnetization. We derive the resulting scaling laws of the QFI in the mean-field and in the high magnetic field limits (HMFL), showing that the SQL can be still circumvented if the variance of magnetization is smaller than N .

The system under consideration is a dilute spin-1 BEC in a homogeneous magnetic field with all three Zeeman states of magnetic quantum number $m_F = 0, \pm 1$. We assume that the single mode approximation (SMA) is valid

and all atoms share the same spatial wavefunction $\phi(\mathbf{r})$ [19, 20] normalized to 1. The Hamiltonian that governs the spin dynamics is [21]

$$\frac{\hat{H}}{\tilde{c}} = \frac{\text{sign}(c_2)}{2N} \hat{J}^2 - q\hat{N}_0, \quad (1)$$

where the energy unit is $\tilde{c} = N|c_2| \int d^3r |\phi(\mathbf{r})|^4$ [22], $c_2 = 4\pi\hbar^2(a_2 - a_0)/3\mu$, μ is an atomic mass, a_0 and a_2 are the s-wave scattering lengths for two spin-1 atoms colliding in the combined symmetric channel, respectively, of spin 0 and 2 [20]. For $c_2 < 0$ the interaction term alone favors the ferromagnetic phase (e.g. rubidium-87), whereas for $c_2 > 0$ the anti-ferromagnetic phase (e.g. sodium-23). The second term in (1) describes the quadratic Zeeman energy, where $q = Q/\tilde{c}$ and $Q = (\mu_B \mathcal{B})^2/(4E_{\text{hf}})$ depends on the magnetic field strength \mathcal{B} , the Bohr magneton μ_B and hyperfine energy splitting E_{hf} which can be both positive and negative [17, 23] (see [22] for corresponding physical parameters). In the Hamiltonian, \hat{J}^2 is the total spin operator and \hat{N}_{m_F} is the particle number operator for the Zeeman state m_F . The total number of atoms and magnetization (the eigenvalue of $\hat{J}_z = \hat{N}_{+1} - \hat{N}_{-1}$) are both conserved and not taken into account in the final form of (1).

In most experiments the system is prepared with a narrow distribution w_M peaked around an average value of magnetization \bar{M} . We assume that the state of the system is [24]

$$\hat{\rho} = \sum_{M=-N}^N w_M \hat{\rho}_M \quad (2)$$

with $\hat{\rho}_M = \hat{P}_M e^{-\beta\hat{H}} \hat{P}_M / \mathcal{Z}_M$, where \hat{P}_M is the projection operator onto the subspace of fixed M , and \mathcal{Z}_M is the statistical sum. We assume that $w_M = \exp[-(M - \bar{M})^2/2\sigma^2]/Z$, where $Z = \sum_M w_M$.

The definition of the QFI follows from quantum estimation theory. The output state $\hat{\rho}_{\text{out}}$ of any linear 3-mode interferometer, with equal phase difference θ between neighboring paths, can be written as $\hat{\rho}_{\text{out}} = e^{-i\theta\hat{\Lambda}_{\mathbf{n}}}\hat{\rho}e^{i\theta\hat{\Lambda}_{\mathbf{n}}}$, where $\hat{\rho}$ is the input density matrix and $\hat{\Lambda}_{\mathbf{n}} = \hat{\Lambda} \cdot \mathbf{n}$, $\hat{\Lambda} = \{\hat{J}_x, \hat{Q}_{zx}, \hat{J}_y, \hat{Q}_{yz}, \hat{D}_{xy}, \hat{Q}_{xy}, \hat{Y}, \hat{J}_z\}$ is a vector of generators [22] spanning the bosonic $SU(3)$ Lie algebra and \mathbf{n} is a unit vector defining the interferometer. The QFI is

$$F_Q[\hat{\rho}, \hat{\Lambda}_{\mathbf{n}}] = 4\mathbf{n}^T \cdot \Gamma[\hat{\rho}] \cdot \mathbf{n}, \quad (3)$$

with the covariance matrix $\Gamma[\hat{\rho}]$ defined as

$$\Gamma_{ij}[\hat{\rho}] = \frac{1}{2} \sum_{k,l} \frac{(p_k - p_l)^2}{p_k + p_l} \text{Re} \left[\langle k | \hat{\Lambda}_i | l \rangle \langle l | \hat{\Lambda}_j | k \rangle \right], \quad (4)$$

where we used eigenvectors and eigenvalues of the input state $\hat{\rho} = \sum p_k |k\rangle \langle k|$. The maximal value of the QFI is given by the largest eigenvalue λ_{max} of the covariance matrix, $F_Q = 4\lambda_{\text{max}}$. The optimal interferometer $\hat{\Lambda}_{\mathbf{n}}$ is

defined by an eigenvector corresponding to λ_{max} . Any separable state gives $F_Q \leq 4N$, while the maximal possible value $F_Q = 4N^2$ occurs only if the quantum state is fully particle entangled. Although for eight generators the covariance matrix (4) has 36 different entries, its form simplifies significantly due to symmetries of $\hat{\rho}$ (for detailed explanation see [22]). The maximal QFI is found to be $F_Q = 4\max(\lambda_A, \lambda_B)$, and

$$\begin{aligned} \lambda_A &= \Gamma_{55} \quad \text{with} \quad \hat{\Lambda}_{\mathbf{n}}^{(A)} = (\hat{D}_{xy} + \alpha\hat{Q}_{xy})/\sqrt{1+\alpha^2}, \quad (5) \\ \lambda_B &= (\Gamma_{11} + \Gamma_{22} + \sqrt{4\Gamma_{12}^2 + (\Gamma_{11} - \Gamma_{22})^2})/2 \quad \text{with} \\ \hat{\Lambda}_{\mathbf{n}}^{(B)} &= [(\hat{J}_x + \gamma\hat{Q}_{zx}) + \alpha(\hat{J}_y + \gamma\hat{Q}_{yz})]/N, \quad (6) \end{aligned}$$

where $\gamma = (\Gamma_{22} - \Gamma_{11} + \sqrt{4\Gamma_{12}^2 + (\Gamma_{11} - \Gamma_{22})^2})/(2\Gamma_{12})$, $N = \sqrt{(1+\alpha^2)(1+\gamma^2)}$ and α is any real number. We found that the diagram of the QFI consists of two regions A and B characterized by the interferometers $\hat{\Lambda}_{\mathbf{n}}^{(A)}$ and $\hat{\Lambda}_{\mathbf{n}}^{(B)}$, respectively. The border between the regions is defined as $\lambda_A(q_t) = \lambda_B(q_t)$, where q_t is the threshold point.

The ground state of the system for $\sigma \rightarrow 0$. In the HMFL one has $\hat{H}/\tilde{c} \approx -q\hat{N}_0$ and all eigenstates are simply given by the Fock states $|N_{+1}, N_0, N_{-1}\rangle$ with the eigenenergies $E(N_0) \approx -qN_0$. For example, in the region A when $q < 0$ the ground state is $|(N+M)/2, 0, (N-M)/2\rangle$ [25] which has the optimal QFI given by $4\lambda_A^{(0)} = 2N^2(1-m^2)$, where $m = |M|/N$ is the positive fractional magnetization. In the region B when $q > 0$ in order to minimize energy one has to maximize occupation of the $m_F = 0$ component, hence the ground state is $|M, N-M, 0\rangle$ for positive M with the QFI equal to $4\lambda_B^{(0)} = 8N^2m(1-m)$. In the non-interacting case ($c_2 = 0$) the border between the regions occurs at $q_t = 0$ where abrupt change of the QFI takes place (the QFI is discontinuous) as a result of transition between λ_A and λ_B .

In both regions, the quasi-distribution functions of the ground state have the shape sketched in Fig. 1 [26], but with different axes defined by an appropriate $SU(2)$ sub-algebra spanned by $\{\tilde{J}_x, \tilde{J}_y, \tilde{J}_z\}$. In the region A the corresponding axes are $\tilde{J}_x = \hat{D}_{xy}$, $\tilde{J}_y = \hat{Q}_{xy}$, $\tilde{J}_z = \hat{J}_z$, while in the region B they are $\tilde{J}_x = (\hat{J}_x + \tilde{\gamma}\hat{Q}_{zx})/\sqrt{2}$, $\tilde{J}_y = (\hat{J}_y + \tilde{\gamma}\hat{Q}_{yz})/\sqrt{2}$, $\tilde{J}_z = (\hat{J}_z + \tilde{\gamma}\sqrt{3}\hat{Y})/2$ with $\tilde{\gamma} = \text{sign}(M)$. The optimal value of the QFI is determined by the interferometer $\hat{\Lambda}_{\mathbf{n}}^{(A)}$ or $\hat{\Lambda}_{\mathbf{n}}^{(B)}$, respectively. As shown in Fig. 1, the Wigner function of the ground state form latitude rings of width 1. Compared to the Bloch sphere radius of length N , this feature is a signature of Heisenberg scaling of the QFI [27]. The maximum of both the Husimi and Wigner distributions is centered around $\langle \tilde{J}_z \rangle$, which is M in the region A and $2M - N$ in the region B .

In the top row of Fig. 2 we show an example of the QFI variation with respect to the parameter q for both anti-ferromagnetic and ferromagnetic interactions obtained

by exact diagonalization of the Hamiltonian (1). The diagram of the QFI consists of two regions A and B , as in the HMFL, but interactions shift the threshold point q_t to positive or negative values of q depending on the interaction sign. Moreover, when the interaction part dominates and $m \geq 0.5$, the QFI is reduced with respect to the HMFL. On the other hand, if $m < 0.5$, one can observe a local maximum in the region B (not presented in Fig. 2). The numerical results can be explained by the mean-field approach [28], which technically means the substitution of bosonic annihilation operators by c-numbers, $\hat{a}_j \rightarrow \sqrt{N} \sqrt{\rho_j} e^{i\theta_j}$. The fraction of atoms ρ_j in the j th component and corresponding angles are then derived by minimization of the mean-field energy functional in the subspace of fixed magnetization [28]. The QFI can be expressed in terms of a single parameter ρ_0 :

$$\frac{F_Q}{4N^2} = \begin{cases} \frac{1}{2} ((1 - \rho_0)^2 - m^2) & \text{for } \rho_0 \leq \rho_t, \\ 2\rho_0(1 - \rho_0) & \text{for } \rho_0 \geq \rho_t, \end{cases} \quad (7)$$

where $\rho_t = (3 - \sqrt{4 + 5m^2})/5$ is the fraction of atoms in the $m_F = 0$ component at the threshold point. In general, $\rho_0 \in (0, 1 - m)$ is also a function of q , and from the numerical study of the relation $\rho_0(q_t) = \rho_t$ we found the approximated formulas for the threshold point q_t : $q_{t-} \approx -1.2$ for $c_2 < 0$ and $q_{t+} \approx 0.8m^2$ for $c_2 > 0$. The above formulas agree within 1% with the threshold points obtained by exact numerical diagonalization. In the bottom row of Fig. 2 we also show eigenvectors corresponding to the maximal eigenvalue of the covariance matrix. Numerical results confirm that for $q < q_{t\pm}$ the eigenvector is $\hat{\Lambda}_n^{(A)}$, while for $q > q_{t\pm}$ it is $\hat{\Lambda}_n^{(B)}$.

The thermal state of the system for $\sigma \rightarrow 0$. The density matrix of the system is $\hat{\rho}_M = \sum_k p_k |k\rangle_M M M |k\rangle$, where $p_k = e^{-\beta \epsilon_{k,M}} / \mathcal{Z}_M$, $\epsilon_{k,M}$ is the dimensionless energy spectrum, $|k\rangle_M$ are eigenstates of the Hamiltonian in the subspace of fixed magnetization M and $\beta = \tilde{c}/k_B T$ accounts for temperature T with k_B being the Boltzmann constant.

In the HMFL $\lambda_{A,B}$ can be approximated by

$$\frac{\lambda_A^{(\beta)}}{N^2} \simeq \frac{1 + \tilde{\beta} + \frac{\tilde{\beta}^2}{2} + \frac{(\tilde{\beta}m)^2}{2}}{\tilde{\beta}^2 (e^{\tilde{\beta}(1-m)} - 1)} - \frac{1 + \tilde{\beta}m}{\tilde{\beta}^2 (1 - e^{-\tilde{\beta}(1-m)})}, \quad (8)$$

$$\frac{\lambda_B^{(\beta)}}{N^2} \simeq \frac{2(1-m)(1 + \tilde{\beta}m)}{\tilde{\beta} (1 - e^{-\tilde{\beta}(1-m)})} - \frac{2 + \tilde{\beta} + \tilde{\beta}m}{\tilde{\beta}^2}, \quad (9)$$

where $\tilde{\beta} = q\beta N$. The threshold point q_t depends on temperature, and one can evaluate it by comparing the leading terms in the Taylor expansions of $\lambda_{A,B}^{(\beta)}$ obtaining $q_t(\beta) \approx -12m/[(1-m)(1+5m)N\beta]$. Apart from the regions A and B we introduce the third one, denoted B' , which appears for any value of q in the high temperature limit $\beta \rightarrow 0$ and in which $\hat{\Lambda}_n^{(B)}$ is still the optimal interferometer. The border between the B and B' regions can be found from an inflection point of (9) which we approximated by $q_{BB'}(\beta) \simeq [\beta N(1-m)]^{-1}$. We find out that in

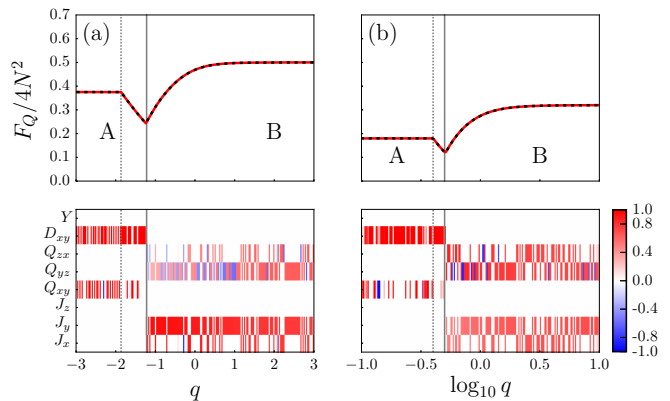


FIG. 2. (Color online) Top row: QFI as a function of q in the ground state of the system for $\sigma \rightarrow 0$, $N = 10^4$ and (a) $c_2 < 0$, $m = 0.5$, (b) $c_2 > 0$, $m = 0.8$. Solid red lines denote numerical results from exact diagonalization of the Hamiltonian in the Fock state basis. Dashed black lines denote mean-field results, as explained in the text. Dashed vertical gray lines mark the position of the critical points $q_c^{(A)} = (1 - \sqrt{1 - m^2})$ for $c_2 > 0$, and $q_c^{(F)} = -(1 + \sqrt{1 - m^2})$ for $c_2 < 0$ [28]. Solid vertical gray lines mark the location of the threshold points $q_{t\pm}$ which separate the regions A and B . Bottom row: eigenvectors corresponding to the largest eigenvalue of the covariance matrix as a function of q , demonstrating the optimal interferometer and confirming the validity of $\hat{\Lambda}_n^{(A,B)}$.

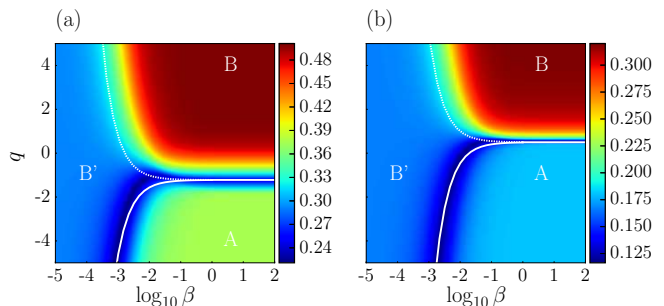


FIG. 3. (Color online) Exact numerical results for $F_Q/4N^2$ as a function of the temperature inverse β and q for $N = 10^3$ (a) $c_2 < 0$, $m = 0.5$, (b) $c_2 > 0$, $m = 0.8$. The solid white line is the border between the A and B , or A and B' , regions which are approximated by $q_t(\beta) + q_{t-}$ for ferromagnetic interactions and $q_t(\beta) + q_{t+}$ for anti-ferromagnetic ones. The dashed white line is the border between the B and B' regions approximated by $q_{BB'}(\beta) + q_{t-}$ in (a) and $q_{BB'}(\beta) + q_{t+}$ in (b).

each of the three regions, away from the borders, the QFI is practically constant and of the order of $O(N^2)$. The landscape of the QFI in the $\beta - q$ plane has the form of three plateaus with the universal values $\lambda_A^{(T=0)}$, $\lambda_B^{(T=0)}$, $\lambda_{B'} = N^2(1-m)(1+5m)/6$ in the regions A , B and B' , respectively.

The interacting system can only be analyzed numerically, except for the case $q = 0$. In Fig. 3 we show the exact results for the QFI as a function of q and β where $c_2 \neq 0$. Indeed, for $\beta \rightarrow 0$, in addition to the A and B

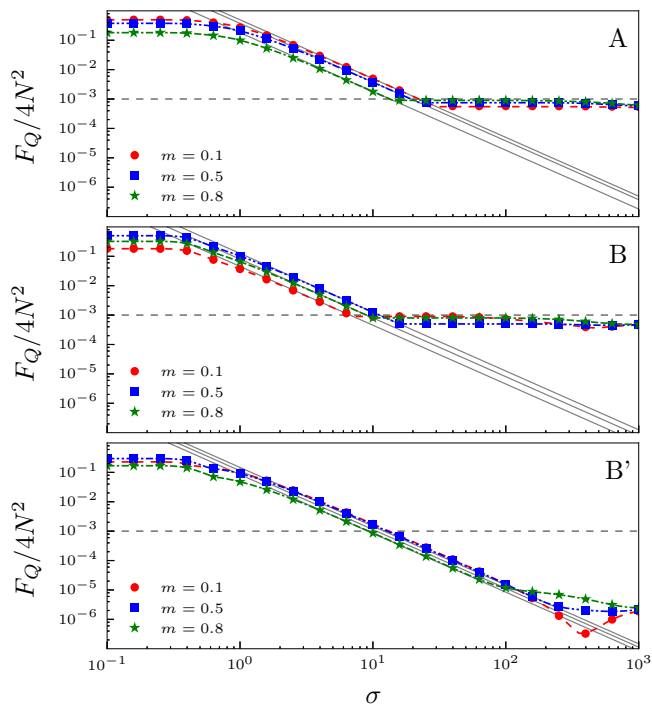


FIG. 4. (Color online) The QFI as a function of σ deeply inside (a) the region A for $q = -10$, $\beta = 100$, (b) the region B for $q = 10$, $\beta = 100$ and (c) the region B' for $q = 10$, $\beta = 10^{-5}$, with $N = 10^3$. Symbols are exact numerical results. Color lines denote numerical results in the HMFL. Gray solid lines denote decay rates, as explained in the text. Gray dashed horizontal lines show the SQL for $N = 10^3$.

regions the third region B' appears. Deeply inside the A , B and B' regions the QFI matches results derived above in the non-interacting limit, corresponding to zero temperature results in A and B , and to the $\beta \rightarrow 0$ result in B' [29]. The borders between particular regions, marked by white lines in Fig. 3, follow the HMFL results with vertical translation $q_{t\pm}$ correcting for the effect of interactions. In all three regions the QFI has the Heisenberg scaling, as we calculated in the HMFL, irrespective of the interaction strength.

Based on simple algebra (see [22]) one can derive the inequality $\lambda_B + 2\lambda_A \geq (\langle \hat{N} \rangle - M)M$, which in the case of macroscopic magnetization means that at least λ_A or λ_B has to scale as $\langle \hat{N} \rangle^2$ even if the total number of atoms fluctuates. The HMFL analysis holds, because for macro-

scopic magnetization all eigenstates of the Hamiltonian remain indeed close to the Fock states.

The thermal state of the system with $\sigma \neq 0$. Increasing the variance of magnetization σ^2 with the Gaussian distribution of w_M strongly reduces the value of the QFI. As in the previous cases, we open discussion with the HMFL case for which decay rates of the QFI can be derived exactly in the regions A , B and B' . Taylor expansion of the covariance matrix (4) around small σ^{-2} (but with fixed N and \bar{M}) gives $\lambda_A(\sigma) \propto \lambda_A^{(0)}(\bar{m})\sigma^{-2}$ in the region A , and $\lambda_B(\sigma) \propto \lambda_B^{(0)}(\bar{m})\sigma^{-2}/4$ in the region B . Eventually for large σ the distribution w_M deviates from the Gaussian and converges to the uniform distribution $w_M \rightarrow 1/(2N)$. In this limit $\lambda_{A,B} \rightarrow 2N$, which is two times smaller than the SQL for the QFI. Similar analysis can be performed deeply inside the region B' , which gives $\lambda_{B'}(\sigma) \propto \lambda_{B'}/(2\sigma^2)$. In Fig. 4 we compare exact numerical results including interactions with the formulas based on the HMFL analysis; good agreement is observed. In general, based on the Taylor expansion of the factors in (4) one can expect decay rates of the QFI to be proportional to σ^{-2} . Hence, the minimal required resolution to beat the SQL is $\sigma < \sqrt{N}$, which is at the edge of current experiments with spin-1 gases [30].

Conclusions. Numerical analysis of spin-1 Bose condensates with non-zero magnetization in a homogeneous magnetic field shows that pure ground states and thermal equilibrium states in the subspace of fixed macroscopic magnetization are useful for quantum interferometry due to the Heisenberg scaling of the QFI value. The diagram of the QFI in the $q-\beta$ plane consists of three regions: (i) A and B which reflect the ground state structure in the low temperature limit and (ii) B' in the high temperature limit. The borders between the regions have been estimated from the results in the HMFL corrected by a shift obtained within the mean field approach. We showed that the QFI in all three regions reaches Heisenberg scaling for fixed and macroscopic magnetization even at a finite temperature. If the variance of magnetization σ^2 is smaller than N , then the SQL can be still overcome. We expect that the SQL should be beaten, whenever the Hilbert space is restricted by a conservation law and experimental techniques to a small subspace only.

E.W. acknowledges discussion with F. Gerbier. This work was supported by the Polish National Science Center Grants DEC-2015/18/E/ST2/00760 and 2014/13/D/ST2/01883.

[1] S. L. Braunstein and C. M. Caves, Phys. Rev. Lett. **72**, 3439 (1994).
 [2] P. Hyllus, W. Laskowski, R. Krischek, C. Schwemmer, W. Wieczorek, H. Weinfurter, L. Pezzé, and A. Smerzi, Phys. Rev. A **85**, 022321 (2012).
 [3] G. Tóth, Phys. Rev. A **85**, 022322 (2012).
 [4] L. Pezzé and A. Smerzi, in *Atom Interferometry (Pro-*

ceedings of the International School of Physics) (Societa Italiana di Fisica, 2014).
 [5] S. L. Braunstein and C. M. Caves, Phys. Rev. Lett. **72**, 3439 (1994).
 [6] H. Strobel, W. Muessel, D. Linnemann, T. Zibold, D. B. Hume, L. A. Pezzé, Smerzi, and M. K. Oberthaler, Science **345**, 424 (2014).

- [7] P. Hauke, M. Heyl, L. Tagliacozzo, and P. Zoller, *Nat. Phys.* **12**, 772 (2016).
- [8] C. Gross, T. Zibold, E. Nicklas, J. Estève, and M. K. Oberthaler, *Nature* **464**, 1165 (2010).
- [9] M. Riedel, P. Böhi, Y. Li, T. W. Hänsch, A. Sinatra, and P. Treutlein, *Nature* **464**, 1170 (2010).
- [10] Z. Zhang and L.-M. Duan, *Phys. Rev. Lett.* **111**, 180401 (2013).
- [11] L.-N. Wu and L. You, *Phys. Rev. A* **93**, 033608 (2016).
- [12] D. Kajtoch and E. Witkowska, *Phys. Rev. A* **93**, 023627 (2016).
- [13] D. M. Stamper-Kurn and M. Ueda, *Rev. Mod. Phys.* **85**, 1191 (2013).
- [14] C. D. Hamley, C. S. Gerving, T. M. Hoang, E. M. Bookjans, and M. S. Chapman, *Nat. Phys.* **8**, 305 (2012).
- [15] M. Gabbriellini, L. Pezzé, and A. Smerzi, *Phys. Rev. Lett.* **115**, 163002 (2015).
- [16] B. Lücke, M. Scherer, J. Kruse, L. Pezzé, F. Deuretzbacher, P. Hyllus, O. Topic, J. Peise, W. Ertmer, J. Arlt, L. Santos, A. Smerzi, and C. Klempt, *Science* **334**, 773 (2011).
- [17] X.-Y. Luo, Y.-Q. Zou, L.-N. Wu, Q. Liu, M.-F. Han, M. Khoon Tey, and L. You, *Science* **355**, 620 (2017).
- [18] J. P. Dowling, G. S. Agarwal, and W. P. Schleich, *Phys. Rev. A* **49**, 4101 (1994).
- [19] C. K. Law, H. Pu, and N. P. Bigelow, *Phys. Rev. Lett.* **81**, 5257 (1998).
- [20] S. Yi, O. E. Müstecaplıođlu, C. P. Sun, and L. You, *Phys. Rev. A* **66**, 011601 (2002).
- [21] R. Barnett, J. D. Sau, and S. Das Sarma, *Phys. Rev. A* **82**, 031602 (2010).
- [22] See Supplemental material.
- [23] F. Gerbier, A. Widera, S. Fölling, O. Mandel, and I. Bloch, *Phys. Rev. A* **73**, 041602 (2006).
- [24] V. Corre, T. Zibold, C. Frapolli, L. Shao, J. Dalibard, and F. Gerbier, *EPL (Europhysics Letters)* **110**, 26001 (2015).
- [25] For simplicity we assume that M and N have the same parity.
- [26] In both cases, $q < 0$ and $q > 0$, one of the m_F states is not occupied, hence the ground states can be mapped onto a two-mode system, for which the quasi-distributions are known.
- [27] L. Pezzé, A. Smerzi, M. Oberthaler, R. Schmied, and P. Treutlein, arXiv:1609.01609.
- [28] W. Zhang, S. Yi, and L. You, *New Journal of Physics* **5**, 77 (2003).
- [29] In region B' , we have $p_n \rightarrow 1$ in Eq. (4), for all n , and based on the orthonormal properties of the Hamiltonian (1) eigenvectors one can also show that $F_Q \simeq N^2(1 - m)(1 + 5m)/6$.
- [30] T. Zibold, V. Corre, C. Frapolli, A. Invernizzi, J. Dalibard, and F. Gerbier, *Phys. Rev. A* **93**, 023614 (2016).

Metrologically useful states of spin-1 Bose condensates with macroscopic magnetization: Supplemental Material

Dariusz Kajtoch,¹ Krzysztof Pawłowski² and Emilia Witkowska¹

¹*Institute of Physics, PAS, Aleja Lotnikow 32/46, PL-02668 Warsaw, Poland*

²*Center for Theoretical Physics, PAS, Aleja Lotnikow 32/46, PL-02668 Warsaw, Poland*

(Dated: December 3, 2024)

I. $SU(3)$ LIE ALGEBRA GENERATORS

A bosonic Lie algebra is constructed from the matrix Schwinger representation:

$$\hat{\Lambda}_\mu = \sum_{m,n=-1,0,+1} (\Lambda_\mu)_n^m \hat{a}_m^\dagger \hat{a}_n, \quad (1)$$

where $(\Lambda_\mu)_n^m$ denotes the m th row and n th column of the matrix Λ_μ . The matrix representation of eight hermitian generators of the $SU(3)$ Lie algebra is given below

$$\begin{aligned} J_x &= \frac{1}{\sqrt{2}} \begin{pmatrix} 0 & 1 & 0 \\ 1 & 0 & 1 \\ 0 & 1 & 0 \end{pmatrix}, & J_y &= \frac{i}{\sqrt{2}} \begin{pmatrix} 0 & -1 & 0 \\ 1 & 0 & -1 \\ 0 & 1 & 0 \end{pmatrix}, \\ J_z &= \begin{pmatrix} 1 & 0 & 0 \\ 0 & 0 & 0 \\ 0 & 0 & -1 \end{pmatrix}, & Q_{xy} &= i \begin{pmatrix} 0 & 0 & -1 \\ 0 & 0 & 0 \\ 1 & 0 & 0 \end{pmatrix}, \\ Q_{yz} &= \frac{i}{\sqrt{2}} \begin{pmatrix} 0 & -1 & 0 \\ 1 & 0 & 1 \\ 0 & -1 & 0 \end{pmatrix}, & Q_{zx} &= \frac{1}{\sqrt{2}} \begin{pmatrix} 0 & 1 & 0 \\ 1 & 0 & -1 \\ 0 & -1 & 0 \end{pmatrix}, \\ D_{xy} &= \begin{pmatrix} 0 & 0 & 1 \\ 0 & 0 & 0 \\ 1 & 0 & 0 \end{pmatrix}, & Y &= \frac{1}{\sqrt{3}} \begin{pmatrix} 1 & 0 & 0 \\ 0 & -2 & 0 \\ 0 & 0 & 1 \end{pmatrix}. \end{aligned} \quad (2)$$

II. COVARIANCE MATRIX

Physical quantities such as the covariance matrix

$$\Gamma_{ij} = \frac{1}{2} \sum_{l,m} \frac{(p_l - p_m)^2}{p_l + p_m} \text{Re} \left[\langle l | \hat{\Lambda}_i | m \rangle \langle m | \hat{\Lambda}_j | l \rangle \right], \quad (3)$$

do not depend on the representation of the Hilbert space. All eigenstates $|k\rangle$ of the system's density matrix $\hat{\rho}$ have the following property:

$$e^{-i\varphi \hat{J}_z} |k\rangle = e^{-i\varphi M} |k\rangle. \quad (4)$$

Rotation of any eigenstate around the \hat{J}_z operator results in a phase factor. It follows that $\Gamma[\hat{\rho}] = \Gamma[\hat{\rho}_\varphi]$, with $\hat{\rho}_\varphi = e^{-i\varphi \hat{J}_z} \hat{\rho} e^{i\varphi \hat{J}_z}$. On the other hand, one can rotate operators rather than the density matrix operator. Equivalently, we can write

$$\Gamma[\hat{\rho}_\varphi] = M_\varphi \cdot \Gamma[\hat{\rho}] \cdot M_\varphi^T. \quad (5)$$

For the order of generators defined by $\hat{\Lambda} = \{\hat{J}_x, \hat{Q}_{zx}, \hat{J}_y, \hat{Q}_{yz}, \hat{D}_{xy}, \hat{Q}_{xy}, \hat{Y}, \hat{J}_z\}$ the rotation matrix M_φ is given by

$$\begin{pmatrix} \cos \varphi & 0 & -\sin \varphi & 0 & 0 & 0 & 0 & 0 \\ 0 & \cos \varphi & 0 & -\sin \varphi & 0 & 0 & 0 & 0 \\ \sin \varphi & 0 & \cos \varphi & 0 & 0 & 0 & 0 & 0 \\ 0 & \sin \varphi & 0 & \cos \varphi & 0 & 0 & 0 & 0 \\ 0 & 0 & 0 & 0 & \cos 2\varphi & -\sin 2\varphi & 0 & 0 \\ 0 & 0 & 0 & 0 & \sin 2\varphi & \cos 2\varphi & 0 & 0 \\ 0 & 0 & 0 & 0 & 0 & 0 & 1 & 0 \\ 0 & 0 & 0 & 0 & 0 & 0 & 0 & 1 \end{pmatrix}. \quad (6)$$

Combining everything we get the condition for the covariance matrix. $\Gamma[\hat{\rho}] = M_\varphi \cdot \Gamma[\hat{\rho}] \cdot M_\varphi^T$. The above condition together with the definition of the covariance matrix and real domain of the Hamiltonian results in the following relations among only nonzero elements $\Gamma_{11} = \Gamma_{33}$, $\Gamma_{55} = \Gamma_{66}$, $\Gamma_{23} = -\Gamma_{14}$, $\Gamma_{22} = \Gamma_{44}$, $\Gamma_{34} = \Gamma_{12}$, and $\Gamma_{77} \neq 0$. Finally, the covariance matrix takes a block diagonal structure

$$\Gamma[\hat{\rho}] = \Gamma_0 \oplus \Gamma_0 \oplus [\Gamma_{55}] \oplus [\Gamma_{55}] \oplus [\Gamma_{77}] \oplus [0], \quad (7)$$

where

$$\Gamma_0 = \begin{pmatrix} \Gamma_{11} & \Gamma_{12} \\ \Gamma_{12} & \Gamma_{22} \end{pmatrix}. \quad (8)$$

The maximal eigenvalue λ_{\max} and the associated eigenvector \mathbf{n} of the covariance matrix form a set which maximizes the QFI, i.e. $F_Q[\hat{\rho}, \hat{\Lambda}_\mathbf{n}] = 4\lambda_{\max}$. Below we list all possible eigenvalues and eigenvectors of the covariance matrix:

- 1) $\lambda_A = \Gamma_{55}$ (double degenerate). The corresponding operator is

$$\hat{\Lambda}_\mathbf{n}^{(A)} = \frac{(\hat{D}_{xy} + \alpha \hat{Q}_{xy})}{\sqrt{1 + \alpha^2}}.$$

- 2) $\lambda_B = (\Gamma_{11} + \Gamma_{22} + \sqrt{4\Gamma_{12}^2 + (\Gamma_{11} - \Gamma_{22})^2})/2$ (double degenerate). The corresponding operator is

$$\hat{\Lambda}_\mathbf{n}^{(B)} = \frac{[(\hat{J}_x + \gamma \hat{Q}_{zx}) + \alpha(\hat{J}_y + \gamma \hat{Q}_{yz})]}{\sqrt{(1 + \alpha^2)(1 + \gamma^2)}}.$$

- 3) $\lambda_C = \Gamma_{77}$. The corresponding operator is $\hat{\Lambda}_\mathbf{n}^{(C)} = \hat{Y}$.

- 4) $\lambda_D = (\Gamma_{11} + \Gamma_{22} - \sqrt{4\Gamma_{12}^2 + (\Gamma_{11} - \Gamma_{22})^2})/2$ (double degenerate). The corresponding operator is

$$\hat{\Lambda}_{\mathbf{n}}^{(D)} = \frac{[(\hat{J}_x + \gamma_D \hat{Q}_{zx}) + \alpha(\hat{J}_y + \gamma_D \hat{Q}_{yz})]}{\sqrt{(1 + \alpha^2)(1 + \gamma_D^2)}}$$

where $\gamma = (\Gamma_{22} - \Gamma_{11} + \sqrt{4\Gamma_{12}^2 + (\Gamma_{11} - \Gamma_{22})^2})/(2\Gamma_{12})$, $\gamma_D = (\Gamma_{22} - \Gamma_{11} - \sqrt{4\Gamma_{12}^2 + (\Gamma_{11} - \Gamma_{22})^2})/(2\Gamma_{12})$ and α is real. Notice that $\lambda_B \geq \lambda_D$. We have checked that $\lambda_C = \lambda_A$ for $q \rightarrow 0$ and $M \rightarrow 0$, and $\lambda_C < \lambda_A$ for other cases. The optimal QFI is then given by $F_Q = 4 \max(\lambda_A, \lambda_B)$.

III. THE INEQUALITY $2\lambda_A + \lambda_B > O(N^2)$

We assume that the state of the system is $\hat{\rho}_M = \hat{P}_M e^{-\beta \hat{H}} \hat{P}_M / \mathcal{Z}_M$, where \hat{P}_M is the projection operator

$$\lambda_B + 2\lambda_A \geq \frac{1}{2}(\Gamma_{11} + \Gamma_{22}) + \Gamma_{12} + 2\Gamma_{55} = \langle (\hat{N} - M)(\hat{N} + M - \hat{N}_0) \rangle \geq (\langle \hat{N} \rangle - M)M. \quad (13)$$

When the magnetization M is fixed and macroscopic, i.e. $M = O(N)$ and $N - M = O(N)$, then either λ_A or λ_B has to be of order N^2 . Consequently, the QFI has to have the Heisenberg scaling $O(N^2)$ even if the total number of atoms fluctuates.

IV. EXPERIMENTAL PARAMETERS

In the following we present examples of physical parameters that are based on the standard Thomas-Fermi approximation (TFA). In the TFA one has $|\phi(\mathbf{r})|^2 = \mu\omega^2(r_{TF}^2 - r^2)/(2c_0N)$ with the TF radius $r_{TF}^5 = 15Nc_0/(4\pi\mu\omega^2)$. The energy unit used in the Letter expressed in terms of the TF radius is

$$\tilde{c} = \frac{2|c_2|}{7c_0} \left(\frac{r_{TF}}{a_{ho}} \right)^2 \hbar\omega, \quad (14)$$

where $a_{ho} = \sqrt{\hbar/\mu\omega}$. The associated coefficient $q = Q/\tilde{c}$ in the Zeeman energy is determined by $Q =$

onto the subspace of fixed M , and \mathcal{Z}_M is the statistical sum. When the magnetization is fixed then by keeping terms of order $O(N^2)$ one has:

$$\Gamma_{11} \approx \langle \hat{N}_0(\hat{N} - \hat{N}_0) \rangle + \frac{1}{2} \left(\langle \hat{a}_0^2 \hat{a}_{-1}^\dagger \hat{a}_1^\dagger \rangle + c.c. \right), \quad (9)$$

$$\Gamma_{22} \approx \langle \hat{N}_0(\hat{N} - \hat{N}_0) \rangle - \frac{1}{2} \left(\langle \hat{a}_0^2 \hat{a}_{-1}^\dagger \hat{a}_1^\dagger \rangle + c.c. \right), \quad (10)$$

$$\Gamma_{12} \approx M \langle \hat{N}_0 \rangle, \quad (11)$$

$$\Gamma_{55} \approx \langle (\hat{N} - \hat{N}_0)^2 - M^2 \rangle, \quad (12)$$

where \hat{N}_0 is the operator of the number of atoms in the $m_F = 0$ component and \hat{a}_{m_F} is the annihilator operator of the atom in the m_F component. By using $\lambda_B \geq \frac{1}{2}(\Gamma_{11} + \Gamma_{22}) + \Gamma_{12}$ and $\hat{N} - \hat{N}_0 > 0$ one can show that

$(\mu_B \mathcal{B})^2/(4E_{hf})$, that is, $Q \approx h(\mathcal{B}/G)^2 277\text{Hz}$ for sodium and $Q \approx h(\mathcal{B}/G)^2 72\text{Hz}$ for rubidium atoms.

Particular parameters calculated in SI units for $N = 10^3$ atoms placed in the symmetric 3D trap with the frequency $\omega/(2\pi) = 300\text{Hz}$ are:

(i) **Sodium-23**: $\tilde{c}/\hbar \approx 70\text{Hz}$; $q = 1$ gives the magnetic field $\mathcal{B} \approx 0.2\text{G}$; $\beta = 1$ gives the temperature $T \approx 0.53\text{nK}$ with $k_B T/\hbar\omega \approx 0.037$. In addition, $q \in (0, 5)$ corresponds to $\mathcal{B} \in (0, 0.45)\text{G}$, while $\beta \in (10^{-3}, 10^2)$ to $T \in (533, 5.3 \times 10^{-3})\text{nK}$.

(ii) **Rubidium-87**: $\tilde{c}/\hbar \approx 17\text{Hz}$; $q = 1$ gives the magnetic field $\mathcal{B} \approx 0.2\text{G}$; $\beta = 1$ gives the temperature $T \approx 0.13\text{nK}$ with $k_B T/\hbar\omega \approx 0.01$. In addition, $q \in (0, 5)$ corresponds to $\mathcal{B} \in (0, 0.44)\text{G}$, while $\beta \in (10^{-3}, 10^2)$ to $T \in (133, 1.3 \times 10^{-3})\text{nK}$.

Other parameters can be taken from [1, 2].

[1] F. Y. Lim and W. Bao, Phys. Rev. E **78**, 066704 (2008).

[2] B. J. Dabrowska-Wüster, E. A. Ostrovskaya, T. J. Alexander, and Y. S. Kivshar, Phys. Rev. A **75**, 023617 (2007).